Monthly Notices of the ROYAL ASTRONOMICAL SOCIETY

MNRAS **534,** 2314–2327 (2024) https://doi.org/10.1093/mnras/stae2200
Advance Access publication 2024 September 25

Exploring M_{BH}–P scaling relations in spiral galaxies: a comparative analysis of inner and outer arm structures

Sanjaya Hettiarachchi,[1,2]★ Prabath Hewageegana[2] and Shameer Abdeen[3]

[1]*Department of Physics, University of Arkansas, Fayetteville, AR 72701, USA*
[2]*Faculty of Science, Department of Physics,University of Kelaniya, Dalugama, Kelaniya 11600, Sri Lanka*
[3]*Department of Physics and Astronomy, Georgia State University, Atlanta, GA 30303, USA*

Accepted 2024 August 31. Received 2024 August 31; in original form 2024 March 6

ABSTRACT

We study the galactic spiral arm pitch angle dependence with wavelength as predicted by the density wave theory. A sample of 10 barred and unbarred spiral galaxies with two distinct, well-defined arms is used for the measurements. The data sample consists of galaxies with inner arms and galaxies with both inner and outer arms. We use six wavebands, namely 3.6 μm, 8.0 μm, *B* band, Hα, H I, and CO for the image analysis. The pitch angles are visually measured with the PYTHON-OL SCRIPT and more precise measurements are obtained using SPIRALITY. We find a 1:1 correlation between pitch angle measurements in the 3.6 and 8.0 μm bands. We predict supermassive black hole (SMBH) masses for 3.6 μm waveband pitch angles using a standard scaling relation. We find that the black hole mass of a galaxy with both inner and outer arms is determined by the average pitch angle of the inner arms. Using only galaxies with inner arms, we find an SMBH mass–pitch angle relation of $\log(M_{\rm BH}/{\rm M}_{\odot}) = (7.11 \pm 0.33) + (0.003 \pm 0.017)P$. Using only galaxies with both inner and outer arms, we find an SMBH mass–pitch angle relation of $\log(M_{\rm BH}/{\rm M}_{\odot}) = (7.56 \pm 0.28) - (0.038 \pm 0.013)P$.

Key words: black hole physics – techniques: image processing – galaxies: formation – galaxies: fundamental parameters – galaxies: spiral – galaxies: structure.

1 INTRODUCTION

The idea of density waves was first introduced by Lindblad (1940, 1942, 1948, 1950), Lindblad & Langebartel (1953), and Lindblad (1961). Moreover, Lindblad's work on kinematic spiral density waves predicts the possibility of forming density waves. His work demonstrates that spirals are formed by dispersion of test particles without self-gravity along particular orbits (dispersion orbits) (Lindblad 1955, 1957, 1958a, b; Lindblad & Langebartel 1956). The classical density wave theory was developed by Lin & Shu (1964), Lin & Shu (1966), Bertin & Lin (1996), and Shu (2016), and later supported observationally by numerous studies (Schweizer 1976; Visser 1980; Gnedin, Goodman & Frei 1995; Grosbøl, Patsis & Pompei 2004; Chemin et al. 2006; Shetty et al. 2007; Zibetti, Charlot & Rix 2009). It was an attempt to overcome the winding problem and to explain the spiral arm structure (Lindblad 1963, 1964; Roberts Jr 1975; Roberts, Roberts & Shu 1975; Rohlfs 1977; Lin & Shu 1987; Bertin et al. 1989a, b; Bertin 2014, 1993; Fuchs 1991, 2000; Bertin & Lin 1996). They proposed that the spiral arms themselves contain no 'permanent' matter and the spiral structure was considered as a quasi-stationary density wave pattern. Since the wave pattern is not attached to any particular piece of the galactic disc, this model avoids the differential rotation problem.

The density wave theory makes a salient prediction that the spiral arm pitch angle (P) should vary with the wavelength of the galaxy image. This variation occurs because stars and gas clouds (gas and dust) exhibit differential rotation, while the spiral arm maintains a uniform global pattern speed ($\Omega_{\rm gp}$). This can be explicitly explained by defining the co-rotation radius ($R_{\rm c}$), where stars and gas clouds orbit the galaxy at the same rate as the spiral arms. Generally, rotation speed of the stars (Ω) is greater than the global pattern speed (i.e. $\Omega > \Omega_{\rm gp}$) inside the co-rotation radius ($R_{\rm c}$). Outside this radius, the rotation speed of the stars is less than the global pattern speed ($\Omega < \Omega_{\rm gp}$). According to the density wave theory, stars form in galactic spiral arms and move away from the density wave as they age. Consequently, the pitch angle's wavelength dependence becomes evident, manifesting as an offset between the spiral arms in different wavelengths. This well-known result is extensively discussed in the literature (e.g. Davis 2015a; Pour-Imani 2018; Miller et al. 2019; Abdeen 2021), yet there are inconsistencies between studies on pitch angle measurements. Most of the existing studies quote galactic pitch angles on a broad scale providing an average pitch angle for galaxies, yet they fail to observe the subtle pitch angle variations between different spiral arms. This study aims to address this by measuring pitch angles focusing on each spiral arm separately and compare them with the existing results.

The choice of the wavelength also plays a pivotal role in these studies. Hence, each wavelength for this study was carefully selected to depict specific components of the spiral. These components trace important stages in the stellar evolution cycle. Although most

★ E-mail: sanjayapraveen2536@gmail.com

existing work focuses on a few selected wavelengths, the lack of existing studies on wavelengths such as H I, H α, and CO led us to incorporate these important wavelengths in our study. Moreover, we find correlations between pitch angles measured in the 8.0 μm waveband and pitch angles measured in B, 3.6 μm, and H α wavebands based on the availability of data.

JWST (Gardner et al. 2023; McElwain et al. 2023; Menzel et al. 2023) data can be used for pitch angle measurements and have the potential to significantly improve results. *JWST* offers significantly higher spatial resolution compared to previous space telescopes. This enhanced resolution allows for more precise identification and measurement of the spiral arms' structure (e.g. Hensley 2023; Lee et al. 2023; Sandstrom et al. 2023), which is crucial for accurate pitch angle determination. Its ability to observe in the infrared spectrum is particularly beneficial for studying spiral galaxies (e.g. Evans et al. 2022; Peltonen et al. 2024). Infrared observations can penetrate dust clouds that often obscure the central regions of galaxies in optical wavelengths, and this capability can reveal the full extent of spiral arms, providing a more complete and accurate measurement of pitch angles. *JWST*'s superior sensitivity enables it to detect fainter structures within galaxies that might be missed by other telescopes (e.g. Whitmore et al. 2023). This can help in identifying subtle features of the spiral arms and their correlation with galactic properties like the SMBH mass. Additionally, *JWST* can provide multiwavelength data, allowing for a more thorough analysis of the galaxies' morphology. This comprehensive data set can improve the robustness of pitch angle measurements by cross-verifying results across different wavelengths. Moreover, with its advanced imaging capabilities, more sophisticated analytical techniques can be applied to the data, leading to potentially new insights and more refined measurements of pitch angles and their correlations with other galactic parameters.

After finding the existence of supermassive black holes (SMBH) as a ubiquitous and an integral part of galactic bulges (e.g. Kormendy & Richstone 1995; Magorrian et al. 1998; Barth 2003; Kormendy 2004), successful efforts have been made to estimate the mass of the SMBHs (M_{BH}). Moreover, studies have affirmed that there are correlations between the SMBH mass and the number of measurable features of the host galaxy. Even though many of the correlating features of the host galaxy require spectroscopic measurements, one which does not is the galactic spiral arm pitch angle. Estimating the SMBH masses solely from imaging data is made feasible by this correlation. It is demonstrated that the spiral arm pitch angle is correlated to the shear rate in galactic discs (Block et al. 1999; Seigar, Block & Puerari 2004; Seigar et al. 2005, 2006, 2014; Grand, Kawata & Cropper 2013; Michikoshi & Kokubo 2014; Kendall, Clarke & Kennicutt Jr 2015; Font et al. 2019; Yu & Ho 2019). The correlation between spiral arm pitch angle and shear rate emphasizes that the tightness of the spiral arms is related to the central mass concentration. In most spiral galaxies, the central mass is dominated by the bulge mass (Seigar 2017) (Hubble type is correlated to the bulge mass (Yoshizawa & Wakamatsu 1975; Graham & Worley 2008). Thus, there is a confirmed correlation between spiral arm pitch angle and bulge mass (Davis et al. 2015). Moreover, the relationship between the bulge mass and the SMBH mass is widely established, as a result of observed correlations of black hole mass with both bulge velocity dispersion and bulge luminosity. Hence, we can assume a relationship between the SMBH mass and the spiral arm pitch angle (Seigar et al. 2008; Berrier et al. 2013; Davis, Graham & Seigar 2017).

The Illustris simulation – a comprehensive cosmological hydrodynamical simulation (Genel et al. 2014) – has been used to study and verify this relationship. The Illustris simulation includes a broad range of astrophysical processes: gas cooling, star formation, and feedback from supernovae and active galactic nuclei, making it an ideal tool for studying galaxy formation and evolution. Analysis of spiral galaxies within the Illustris simulation demonstrates a strong correlation between the spiral arm pitch angle and the SMBH mass, consistent with observational data. Specifically, the simulation predicts a slope and normalization of -0.055 ± 0.001 and 8.40 ± 0.01 for the log ($M_{BH}/M_{\odot}$)–P relation, respectively (Mutlu-Pakdil et al. 2018), closely aligning with the empirical findings of Berrier et al. (2013). These results confirm that the Illustris simulation replicates the observed pitch angle–SMBH mass relation, reinforcing the idea that pitch angle can serve as a reliable proxy for estimating SMBH mass in disc galaxies. This connection provides a valuable tool for investigating SMBHs in galaxies where direct mass measurements are challenging.

The correlation between SMBH mass and spiral arm pitch angle in galaxies, while insightful, is subject to several limitations and uncertainties. Measurement uncertainties in pitch angle due to varying imaging data quality and methods can directly impact the accuracy of the estimated SMBH mass. Additionally, sample selection bias, particularly favouring well-defined spiral structures, may not represent the diversity of all spiral galaxies. The inherent scatter in the correlation further complicates the relationship, as various factors influence both SMBH mass and spiral structure. The correlation's strength varies with galaxy type and is influenced by the bulge-to-disc ratio, with bulge-dominated galaxies showing a stronger correlation to disc-dominated ones. Moreover, the correlation might evolve with redshift, as galaxy properties change over cosmic time, and be affected by environmental factors, such as galaxy interactions or the presence of a cluster. Non-linearities and higher order effects may also play a role, indicating that the relationship might not be strictly linear and that additional variables could influence the correlation.

In this paper, we calculate SMBH masses using a refined M_{BH} –P relation from Berrier et al. (2013), and compare them with the existing results. For galaxies with inner and outer spiral arms, the literature also fails to distinguish the effects due to each arm type when calculating black hole masses using scaling relations. Based on our data sample, we show that the black hole mass of a galaxy with inner and outer arms is governed by the average pitch angle of the inner arms. The existing M_{BH}–P relations focus only on the prominent inner arm structures, yet it is important to study these relations in a broader context with both inner and outer arm structure measurements. This study investigates the inner and outer spiral arm pitch angles separately and discusses the effects of the pitch angle choice in the M_{BH}–P relation.

2 THE DATA SAMPLE

We used a sample (see Table 1) of 10 barred and unbarred spiral galaxies with clearly visible, two distinct spiral arms. We confined our study to galaxies with arms that are long, continuous, and symmetric, i.e. mostly grand design spiral galaxies. Since we overlay synthetic logarithmic spirals on the spiral arms, the grand design property plays a pivotal role. Six of the selected galaxies are categorized as arm-class 12 (two long symmetric arms dominating the optical disc grand design), and three of them are under arm-class 9 (two symmetric inner arms, multiple long and continuous outer arms) according to Elmegreen & Elmegreen (1987).

Our galaxy sample can be categorized into two groups. (a) galaxies with inner arms only, namely NGC 1300, NGC 1365, NGC 5194, NGC 7479, and NGC 7552. (b) galaxies with both inner arms and

Table 1. galaxy sample with basic parameters.

galaxy name (1)	Morphology (2)	RA (J2000) (3)	Dec. (J2000) (4)	i° (5)	PA$^\circ$ (6)	Eccentricity (7)	Distance (Mpc) (8)	Method (9)
NGC 1300	SB(rs)bc	03 19 41.085	−19 24 40.9	23.07	106.0	0.391865	14.50	Tully–Fisher
NGC 1365	SB(s)b	03 33 36.3715	−36 08 25.45	32.38	32.0	0.535509	18.10	TRGB
NGC 1566	SAB(s)bc	04 20 00.425	−54 56 16.1	13.10	60.0	0.226666	18.00	Tully–Fisher
NGC 4321	SAB(s)bc	12 22 54.8315	+ 15 49 18.54	9.20	30.0	0.159958	13.90	SNIa
NGC 5194	SA(s)bc pec	13 29 52.7115	+ 47 11 42.62	26.65	163.0	0.448552	7.55	TRGB
NGC 5236	SAB(s)c	13 37 00.9505	−29 51 55.50	14.81	45.0	0.114901	4.90	FGLR
NGC 5248	SAB(rs)bc	13 37 32.0245	+ 08 53 06.64	18.19	110.0	0.312184	14.30	Tully–Fisher
NGC 5364	SA(rs)bc pec	13 56 12.005	+ 05 00 52.1	24.27	30.0	0.411118	13.60	Tully–Fisher
NGC 7479	SB(s)c	23 04 56.655	+ 12 19 22.4	15.60	25.0	0.268970	36.80	Tully–Fisher
NGC 7552	(R')SB(s)ab	23 16 10.7593	−42 35 05.07	13.10	1.0	0.226666	14.80	Tully–Fisher

Notes. Columns: (1) galaxy name. (2) Hubble morphological type. (3) RA (J2000). (4) Dec. (J2000). (5) Inclination angle in degrees derived from equation (1). (6) Position angle in degrees [Source: NASA/IPAC Extragalactic Database (NED)[1]]. (7) Eccentricity [Source: NASA/IPAC Extragalactic Database (NED)]. (8) Distance (Mpc) [Source: NASA/IPAC Extragalactic Database (NED)]. (9) Method used for distance measurements.

[1]The NASA/IPAC Extragalactic Database (NED) is operated by the Jet Propulsion Laboratory, California Institute of Technology, under contract with the National Aeronautics and Space Administration.

outer arms, namely NGC 1566 (Elmegreen et al. 2011), NGC 4321 (Elmegreen et al. 2011), NGC 5236 (Elmegreen & Elmegreen 1987), NGC 5248 (Sandage 1961), and NGC 5364 (Sandage 1961).

Multiwavelength astronomy is an integral part of exploring the universe because observing primarily at a particular wavelength provides a skewed picture of the universe. Looking at galaxies with different wavebands gives us a crystal-clear understanding of their physical processes and concentration. In this work, the galaxies were analysed in six different wavebands, namely *B* band (445 nm), 3.6 μm, 8.0 μm, Hα, CO, and H I according to the availability of data.

Our galaxy sample was confined to a distance of 36.80 Mpc with NGC 7479 having the furthest recorded distance. In this paper, we calculated inclination angles of the galaxy sample using equation (1).

$$i = \cos^{-1}\left(\sqrt{1-e^2}\right), \tag{1}$$

where i is the inclination angle and e stands for eccentricity. We selected our galaxies such that the inclination angles are $<40^\circ$. If the galaxy has a very high inclination angle, most of the cardinal details will be lost in the deprojection process.

3 ANALYSIS

3.1 Image pre-processing

All galaxies are viewed with some inclination. Thus, before measuring the pitch angles, irrespective of the method, all the galaxies had to be deprojected to a face-on orientation. The pitch angle of a logarithmic spiral at any radius is defined as the angle between a line tangent to the spiral and a line tangent to a circle with the same radius and centre as the spiral. The deprojection process presumes that a galaxy with its disc plane parallel to the plane of the sky will appear circular, and a circular galaxy with random inclination will appear on the sky as an ellipse. After deprojection, the resulting image was cropped into a perfect square, as required by *PYTHON-OL SCRIPT* and *spirality*. IRAF[2] (IMAGE REDUCTION AND ANALYSIS FACILITY) software was used for the deprojection and cropping processes.

[2]https://pkgs.org/download/iraf

3.2 Measuring pitch angles

3.2.1 Using the Python-OL script

We initially obtained rough pitch angle measurements using the PYTHON-OL SCRIPT[3] (Python-based code) (SPIRAL_OVERLAY.PY). This Python code provides the capability to load a properly deprojected and cropped FITS image by generating a graphical interface. A synthetic logarithmic spiral can be overlaid on a foreground layer. Pitch angle, phase angle, chirality, and the number of arms are available for variation.

It is a well-established fact that the majority of galaxies have spiral arms that cannot be fitted with a single pitch angle (Savchenko & Reshetnikov 2013; Herrera-Endoqui et al. 2015). Hence, in this method, we measured the pitch angles for each spiral arm separately instead of measuring an average pitch angle. In order to minimize the uncertainty of the pitch angles, we obtained the minimum and maximum pitch angles by tracing the logarithmic spirals twice for each spiral arm separately.

The accuracy of this process strictly depends on the image limpidity of the spiral arms and the arm–interarm contrast. Arm–interarm contrast emphasizes how much brighter the spiral arm is when compared to the adjacent interarm region. Generally, arm–interarm contrast becomes strongest between the inner region and the co-rotation circle and is weaker beyond that (Elmegreen 1998). Since the overlaying synthetic spiral traces are logarithmic, if the actual spiral galaxy structure has intrinsic deviations from being logarithmic, the Python-OL script method would not be accurate.

3.2.2 Using the SPIRALITY

SPIRALITY[4] (Shields et al. 2015, 2022) is a Matlab-based code that can be used to measure pitch angles accurately. The pitch angles were obtained using SPIRALITY; SPIRALITY-CALL-NO-SYMMETRY script. SPIRALITY; SPIRAL-ARM-COUNT script (Shields et al. 2015) has the capability of fitting synthetic logarithmic spirals over the actual image spiral arms pursuant to the brightest pixels, and it measures the

[3]https://github.com/ebmonson/2DFFTUtils-Module
[4]https://ascl.net/assets/codes/Spirality/Spirality.zip

number of spiral arms in a given spiral galaxy image. In this method, we measured the pitch angles for each spiral arm separately. Since the entire process is automated, this method minimizes the user bias in tracing the logarithmic spirals and measuring the pitch angles.

4 RESULTS

4.1 Pitch angle measurements

The pitch angles were measured for both spiral arms separately using the SPIRALITY (see Table 2). We calculated the average pitch angles and compared them with the existing literature values (see Table 3). The northern outer spiral arm of the NGC 1566 has a tight bend, and it intrinsically deviates from being logarithmic. Hence, we used the arm segment indicated by the solid red line to measure the pitch angles (see Fig. 1), and it might significantly affect our pitch angle measurements. For NGC 1566, at the wavelength of 3.6 μm, we measured the pitch angles of the inner arms. We claim the pitch angle of the northern and southern inner arm and their average measurement to be 22.99 ± 0.34°, 21.10 ± 0.56°, and 22.05 ± 0.33°, respectively.

We measured CO waveband pitch angles separately for both inner arms of NGC 4321, but we were unable to find any pitch angle record for the CO waveband in the literature (see Tables 2 and 3). Since we were unable to detect the outer arms of NGC 4321 using our galaxy images corresponding to the available wavelengths, we had to use an optical image to measure the pitch angles. Since the northern outer spiral arm of NGC 4321 is unclear and blurry, we only measured the pitch angles of the southern outer spiral arm, considering the arm segment indicated by the solid red line (see Fig. 2). The pitch angle of the arm segment is 26.69 ± 1.89°.

A remarkable H I distribution of NGC 5236 has been mapped with the Australia Telescope Compact Array (Jarrett et al. 2012) and extends beyond the GALEX XUV disc (Thilker et al. 2007). A large amount of H I exists outside the Holmberg Radius (Huchtmeier & Bohnenstengel 1981). The overall impression of NGC 5236 in neutral hydrogen emphasizes a distorted one-arm spiral (indicating a peculiar outer arm) (see Fig. 3) and implies that it may have interacted or merged with another smaller galaxy (Koribalski et al. 2018). In this study, we claim the H I outer arm pitch angle to be 8.91 ± 0.12°.

Since the outer arms of NGC 5248 are not visible and detectable in our galaxy images corresponding to the available wavelengths, we converted an optical image with visible outer arms to an FITS image. Hence, the outer arm pitch angles were measured using that FITS image. We measured the pitch angle of the northern and southern outer arm and their average measurement to be 11.60 ± 0.14°, 11.31 ± 0.16°, and 11.46 ± 0.11°, respectively.

Since the inner arms of NGC 5364 are clearly visible in the 3.6 μm waveband galaxy images, we measured the 3.6 μm waveband pitch angles of the inner arms. The pitch angles of the northern inner arm, the southern inner arm, and their average are 20.85 ± 0.40°, 25.32 ± 0.18°, and 23.09 ± 0.22°, respectively.

The discrepancies between the northern and southern arm pitch angle measurements of NGC 4321 and NGC 5248 (both are intermediate galaxies) can be attributed to several complex factors. These include intrinsic asymmetries in the spiral structure, which may arise from the gravitational influence of dark matter subhaloes causing tidal forces that distort the spiral arms differently on each side (e.g. Purcell et al. 2011). Additionally, the interaction between spiral density waves and galactic bars or central mass concentrations can lead to variations in pitch angles (Muñoz-Mateos et al. 2015). Differential rotation and shear within the galaxy can cause the spiral arms to experience varying amounts of shear, leading to discrepancies (Lin & Shu 1964). Secular evolution processes, such as bar formation and migration of stars, can alter the structure and then pitch angles of spiral arms over time (Kormendy & Kennicutt Jr 2004). Magnetic fields, with their varying strength and orientation, can influence the formation and maintenance of spiral arms, causing differences in pitch angles between northern and southern arms (Beck 2016). Gas dynamics and feedback from star formation and supernovae can create asymmetries in the arms (Dobbs & Baba 2014). Moreover, observational biases such as differences in viewing angle, resolution, and sensitivity across the galaxy's disc, along with interstellar dust and star formation regions that obscure parts of the galaxy unevenly, may contribute to apparent discrepancies. Temporal evolution of the spiral arms, where different segments may be at different stages of their evolution, leads to variations in pitch angle measurements between the northern and southern arms (Seigar et al. 2008). According to density wave theory, variations in the density wave pattern speed and its coupling with the disc material can cause differences in the pitch angles (Lin & Shu 1964). Non-circular streaming motions of gas within the galaxy, often induced by gravitational interactions or internal instabilities, can further lead to variations in the observed pitch angles (e.g. García-Burillo et al. 2003). These factors combined create the observed differences in pitch angle measurements between the northern and southern arms. Moreover, tidal interactions due to companion galaxies can significantly influence the spiral structure of galaxies, causing subtle differences in pitch angles between their northern and southern spiral arms. For example, NGC 1566 is part of the Dorado Group where tidal interactions between NGC 1566 and neighbouring galaxies could lead to its asymmetries and warps. The interacting galaxy pair NGC 1596/1602 is a possible candidate for such a tidal encounter, potentially contributing to the observed pitch angle differences in its spiral arms. Similarly, NGC 4321, a member of the Virgo Cluster, interacts with nearby galaxies such as NGC 4323 and NGC 4328. These interactions could lead to the observed asymmetry in the pitch angles of its spiral arms. Interestingly, NGC 5194 has a well-documented companion, NGC 5195, which induces tidal forces. However, despite this interaction, there are no considerable differences between the northern and southern arm pitch angles, suggesting other factors might be at play in maintaining the symmetry of its spiral structure.

The observed discrepancy between the northern and southern arm pitch angles of NGC 1300 and NGC 1365 can be attributed to several well-documented factors. Notably, Martínez-García (2011) has analysed the spiral structure of NGC 1300 and identified significant asymmetries between the arms. These asymmetries are often linked to the influence of the galaxy's strong bar structure, which creates varying gravitational potentials that affect the formation and maintenance of spiral arms differently across the northern and southern regions. Supporting this, Elmegreen & Elmegreen (1985) suggest that bars can induce spiral arm asymmetry through their dynamic interactions with the disc, leading to variations in pitch angles. Additionally, simulations by Athanassoula (2012) reinforce the notion that the bar's influence can generate such asymmetries. Consequently, these documented asymmetries are likely responsible for the differing pitch angles observed between the northern and southern arms of NGC 1300 and NGC 1365.

4.2 Comparison with other existing results

We graphically compared our average pitch angle measurements corresponding to each wavelength with the values in the literature based on the availability of data (CO and H I bands were excluded

Table 2. Pitch angle measurements.

galaxy	P° (*B* band)		P° (3.6 μm)		P° (8.0 μm)		P° (Hα)		P° (CO)		P° (H I)	
	Northern	Southern	Northern	Southern	Northern	Southern	Northern	Southern	Northern	Southern	Northern	Southern
NGC 1300	$12.08^{+0.19}_{-0.19}$	$17.09^{+0.36}_{-0.36}$	$9.41^{+0.10}_{-0.10}$	$16.62^{+0.11}_{-0.11}$	–	–	$10.21^{+0.15}_{-0.15}$	$15.61^{+0.39}_{-0.39}$	–	–	–	–
NGC 1365	$25.62^{+0.11}_{-0.11}$	$27.64^{+0.11}_{-0.11}$	$27.17^{+0.30}_{-0.30}$	$32.28^{+0.53}_{-0.53}$	–	–	–	–	–	–	–	–
NGC 7479	–	$10.60^{+0.14}_{-0.14}$	–	$10.62^{+0.13}_{-0.13}$	–	–	–	$10.99^{+0.25}_{-0.25}$	–	–	–	–
NGC 7552	$18.63^{+0.34}_{-0.34}$	–	$18.92^{+0.37}_{-0.37}$	–	$19.15^{+0.50}_{-0.50}$	–	$23.52^{+0.76}_{-0.76}$	–	–	–	–	–
NGC 1566	$17.02^{+0.50}_{-0.50}$	$13.52^{+0.58}_{-0.58}$	$17.13^{+1.09}_{-1.09}$	$15.12^{+0.19}_{-0.19}$	$17.75^{+0.51}_{-0.51}$	$14.18^{+0.68}_{-0.68}$	$17.96^{+0.25}_{-0.25}$	$14.23^{+0.82}_{-0.82}$	–	–	–	–
NGC 4321	$13.02^{+0.16}_{-0.16}$	$18.83^{+0.65}_{-0.65}$	$13.59^{+0.21}_{-0.21}$	$19.88^{+0.27}_{-0.27}$	$13.61^{+0.20}_{-0.20}$	$19.66^{+1.63}_{-1.63}$	$13.27^{+0.23}_{-0.23}$	$20.12^{+0.76}_{-0.76}$	$15.77^{+0.73}_{-0.73}$	$19.88^{+1.69}_{-1.69}$	–	–
NGC 5194	$13.06^{+0.37}_{-0.37}$	$11.76^{+0.87}_{-0.87}$	$11.49^{+0.86}_{-0.86}$	$11.64^{+2.09}_{-2.09}$	$11.49^{+1.00}_{-1.00}$	$11.94^{+1.07}_{-1.07}$	$11.10^{+0.99}_{-0.99}$	$11.39^{+1.79}_{-1.79}$	$13.04^{+0.14}_{-0.14}$	$12.35^{+0.33}_{-0.33}$	$12.95^{+0.53}_{-0.53}$	$13.36^{+1.65}_{-1.65}$
NGC 5236	$14.02^{+0.43}_{-0.43}$	$13.06^{+0.30}_{-0.30}$	$14.18^{+0.24}_{-0.24}$	$14.17^{+0.79}_{-0.79}$	$14.55^{+0.17}_{-0.17}$	$14.07^{+0.87}_{-0.87}$	$14.27^{+0.14}_{-0.14}$	$14.47^{+0.82}_{-0.82}$	–	–	–	–
NGC 5248	$25.78^{+0.14}_{-0.14}$	$35.43^{+0.29}_{-0.29}$	$24.84^{+0.35}_{-0.35}$	$36.24^{+0.61}_{-0.61}$	–	–	$23.63^{+0.64}_{-0.64}$	$35.06^{+0.46}_{-0.46}$	–	–	–	–
NGC 5364	$10.09^{+0.50}_{-0.50}$	$10.79^{+0.31}_{-0.31}$	$10.87^{+0.43}_{-0.43}$	$10.33^{+0.87}_{-0.87}$	–	–	–	–	–	–	–	–

Notes. Northern and southern spiral arm pitch angles in degrees from the SPIRALITY for different wavebands as shown in the table. The first section lists barred spiral galaxies, while the second section lists intermediate and unbarred spiral galaxies.

due to lack of data), as shown in Fig. 4. There are two main reasons for the discrepancies between our pitch angle measurements and the values in the literature. The first reason is related to the differences in the deprojecting parameters (inclination, eccentricity, and position angle). The parameter causing the most trouble is clearly the galaxy's inclination. In this study, we report the *B*-band and 8.0 μm average pitch angles of the outer arms of NGC 1566 to be 15.27 ± 0.38° and 15.97 ± 0.43°, respectively, while Miller et al. (2019) recorded 31.20 ± 4.80° and 44.13 ± 11.94°. A simple inspection of NGC 1566 image shows that the spiral arms are symmetric and quite similar in the *B*-band and 8.0 μm wavelengths. Thus, such a larger discrepancy in pitch angles is questionable. These discrepancies are mainly due to differences in the galaxy's inclination. For NGC 1566, we used an inclination of 13.10°, while Miller et al. (2019) had used 34.3°. For NGC 5248, at the *B* band, we measured the northern and southern inner arm pitch angles to be 25.78 ± 0.14° and 35.43 ± 0.29°, respectively, while Ma (2001) reported 23.8° and 22.7°. These sharp disagreements of pitch angles are basically due to differences in the inclination angle. For NGC 5248, we used an inclination of 18.19°, while Ma (2001) had used 43.7°. Moreover, in Ma (2001), there are uncertainties in measuring the pitch angles of the spiral arms and inclination angles due to the uncertainties of sampling the points on the central line of the mass of the spiral arm. For NGC 7552, at wavelengths of *B* band, 3.6 μm, and 8.0 μm, we measured the average pitch angles values to be 18.63 ± 0.34°, 18.92 ± 0.37°, and 19.15 ± 0.50°, respectively, while Abdeen (2021) recorded 27.6 ± 3.4°, 25.9 ± 3.7°, and 29.0 ± 2.8°. The most probable reason for these pitch angle disagreements is differences in the inclination angle. According to our parameters, the inclination angle is 13.10°, while Abdeen (2021) records an inclination angle of 19°. Utilizing inclination and position angle values from Abdeen (2021), specifically 19° and -76.98° respectively, we conducted a deprojection of the 3.6 μm waveband image of NGC 7552. Employing these parameters, the SPIRALITY code yielded a pitch angle measurement of 25.42 ± 0.22°. This result is in agreement with the established literature value, thus corroborating the dependence of pitch angle on the inclination angle. This verification underscores the critical importance of precise inclination and position angle inputs in the accurate determination of pitch angles in spiral galaxies. A galaxy that is common to Yu & Ho (2018) and our sample is NGC 7552. In this case there is also a sharp disagreement for the *B*-band and 3.6 μm measurements, since the values given in Yu & Ho (2018) are 9.7 ± 0.9° and 9.7 ± 1.1°, respectively, while our values are 18.63 ± 0.34° and 18.92 ± 0.37°. These discrepancies are mainly due to differences in the position angle and eccentricity. For NGC 7552, we used a position angle and an eccentricity value of 1° and 0.2267, respectively, while Yu & Ho (2018) had used 5° and 0.3919 [calculated using the given ellipticity (0.08) in Yu & Ho (2018)]. However, Yu & Ho (2018) only reports measurements for their 1DFFT method. Their 2DFFT method did not return a value for NGC 7552 due to its long bar. Our SPIRALITY code correctly identified the spiral arm and returned an acceptable pitch angle value corresponding to our deprojecting parameters.

The second reason refers to our pitch angle measurement procedure. We measured the pitch angles for both spiral arms separately and calculated the average pitch angles using them. Most of the literature values indicated in Table 3 represent only an average pitch angle for both arms.

A sharp discrepancy is evident when comparing our average measurement of NGC 1365 in the *B* band, 44.28 ± 0.12°, with the absolute values recorded by Ma (2001), 13.8° and 17.8°. Additionally, we report the 3.6 μm average pitch angle of NGC 1365 to be 29.73 ± 0.30°, while Al-Baidhany et al. (2019) and Díaz-García et al. (2019) recorded 15.4 ± 2.4° and 19.1 ± 5.2°, respectively. These discrepancies may primarily be attributed to the variable pitch angles of NGC 1365. NGC 1365 is a well-documented example of a galaxy with a variable pitch angle (Ringermacher & Mead 2009). This galaxy exhibits a high pitch angle near the junction of the spiral arm and galactic bar, and a lower pitch angle in its outermost regions. In this particular galaxy, we focused on measuring pitch angles predominately in the inner part of the disc. The SPIRALITY code correctly identified the high pitch angles near the galactic bar-spiral arm junction and gave us the required innermost stable pitch angles of the spiral arm.

Furthermore, pitch angles may depend on the method we use when the galaxy image is unclear, the structure is not clearly visible, or when the structure deviates from the logarithmic scale. Thus, different pitch angles may be obtained for the same galaxy, depending on the pitch angle measurement methods. For instance, the northern inner arm of NGC 5236 deviates from being logarithmic. In addition, some branches and feathers are connected to that arm. As a result, SPIRALITY cannot trace the most accurate and reasonable logarithmic spiral to the northern inner arm. These reasons may affect our pitch angle measurements and cause some discrepancies compared to the values in the literature (see Table 3). The spiral arms of NGC 7479 also do not present a clear logarithmic geometry (especially the northern arm). Thus, we only measured the pitch angles of the southern arm, which may cause some discrepancies with the values in the literature (see Table 3). In this study, we report the *B*-band pitch angle of the southern arm of NGC 7479 to be 10.60 ± 0.14°, while Martínez-García (2012) recorded an average

Table 3. Average pitch angle measurements.

galaxy	P° (B band)		P° (3.6 μm)		P° (8.0 μm)		P° (Hα)		P° (CO)		P° (H I)	
	Average	from Lit.	Average	from Lit.	Average	from Lit.	Average	from Lit.	Average	from Lit.	Average	from Lit.
NGC 1300	$14.59^{+0.20}_{-0.20}$	$-12.71^{+1.99}_{-1.99}$ [1] $13.1^{+7.7}_{-0.3}$ [2] 12.1, 11.0 [3] $31.7^{+1.1}_{-1.1}$ [4] $10.3^{+1.8}_{-1.8}$ [5] 14.44 [6] 19.91 [6] 12^{+3}_{-3}[7] $16.0^{+6.5}_{-6.5}$ [7] $23.96^{+1.61}_{-1.61}$ [7]	$13.02^{+0.07}_{-0.07}$	$12.7^{+1.8}_{-1.8}$ [8] $14.7^{+5.4}_{-5.4}$ [9]	–	–	$12.91^{+0.21}_{-0.21}$	–	–	–	–	–
NGC 1365	$26.63^{+0.08}_{-0.08}$	$-34.81^{+2.80}_{-2.80}$ [1] 13.8, 17.8 [3]	$29.73^{+0.30}_{-0.30}$	$15.4^{+2.4}_{-2.4}$ [8] $19.1^{+5.2}_{-5.2}$ [9]	–	–	–	–	–	–	–	–
NGC 1566	$15.27^{+0.38}_{-0.38}$	$18.2^{+1.7}_{-1.7}$ [10] $-17.81^{+3.67}_{-3.67}$ [1] $20.9^{+2.4}_{-2.4}$ [11] $19.8^{+0.6}_{-0.6}$ [11] $31.20^{+4.80}_{-4.80}$ [12]	$16.13^{+0.55}_{-0.55}$	$20.0^{+1.8}_{-1.8}$ [10] $21.4^{+2.3}_{-2.3}$ [11] $20.5^{+0.3}_{-0.3}$ [11] $15.29^{+2.37}_{-2.37}$ [12] $21.31^{+4.78}_{-4.78}$ [8] $26.5^{+7.6}_{-7.6}$ [9]	$15.97^{+0.43}_{-0.43}$	$22.4^{+1.5}_{-1.5}$ [10] $44.13^{+11.94}_{-11.94}$ [12]	$16.10^{+0.43}_{-0.43}$	22^{+2}_{-2} [13] 29.74 [14]	–	–	–	–
NGC 4321	$15.93^{+0.33}_{-0.33}$	$16.1^{+2.8}_{-2.8}$ [10] 21.0, 14.3 [3] 14.2 [15] $15.06^{+1.20}_{-1.20}$ [12] 14.0 [16] 22.7 [16] 18.4 [16]	$16.74^{+0.17}_{-0.17}$	$16.1^{+2.4}_{-2.4}$ [10] $18.60^{+1.69}_{-1.69}$ [12] $21.4^{+5.0}_{-5.0}$ [9]	$16.64^{+0.82}_{-0.82}$	$14.7^{+1.7}_{-1.7}$ [10] $24.46^{+3.76}_{-3.76}$ [12]	$16.70^{+0.40}_{-0.40}$	15^{+3}_{-3} [13] $21.18^{+2.50}_{-2.50}$ [12]	$17.83^{+0.92}_{-0.92}$	–	–	–
NGC 5194	$12.41^{+0.47}_{-0.47}$	$10.2^{+2.7}_{-2.7}$ [10] 16.7, 15.8 [3] 13.9 [16] 13.8 [16]	$11.57^{+1.13}_{-1.13}$	$9.7^{+2.2}_{-2.2}$ [10] $17.1^{+0.6}_{-0.6}$ [9] $14.9^{+2.5}_{-2.5}$ [9]	$11.72^{+0.73}_{-0.73}$	$10.5^{+2.7}_{-2.7}$ [10]	$11.25^{+1.02}_{-1.02}$	15^{+2}_{-2} [13] -11.88 [14] $11.3^{+0.3}_{-0.3}$ [17]	$12.70^{+0.18}_{-0.18}$	–	$13.16^{+0.87}_{-0.87}$	–
NGC 5236	$13.54^{+0.26}_{-0.26}$	$-16.04^{+1.74}_{-1.74}$ [1] 16.6 [16] 17.4 [16]	$14.18^{+0.41}_{-0.41}$	$18.1^{+4.9}_{-4.9}$ [9]	$14.31^{+0.44}_{-0.44}$	–	$14.37^{+0.42}_{-0.42}$	16^{+2}_{-2} [13] 14.04 [14]	–	–	–	–
NGC 5248	$30.61^{+0.16}_{-0.16}$	22.7, 23.8 [3]	$30.54^{+0.35}_{-0.35}$	$23.6^{+6.1}_{-6.1}$ [9]	–	–	$29.35^{+0.39}_{-0.39}$	–	–	–	–	–
NGC 5364	$10.44^{+0.29}_{-0.29}$	8.4 [15]	$10.60^{+0.49}_{-0.49}$	$9.7^{+0.1}_{-0.1}$ [9] $15.5^{+4.1}_{-4.1}$ [9]	–	–	–	–	–	–	–	–
NGC 7479	$10.60^{+0.14}_{-0.14}$	$15.7^{+1.5}_{-1.5}$ [10] $31.5^{+1.6}_{-3.2}$ [2] $17.8^{+1.2}_{-1.2}$ [4] 10.7 [15] 6.8 [16] 10.3 [16]	$10.62^{+0.13}_{-0.13}$	$14.0^{+1.2}_{-1.2}$ [10]	–	–	$10.99^{+0.25}_{-0.25}$	–	–	–	–	–
NGC 7552	$18.63^{+0.34}_{-0.34}$	$27.6^{+3.4}_{-3.4}$ [10] $19.3^{+1.7}_{-1.7}$ [4] $9.7^{+0.9}_{-0.9}$ [11]	$18.92^{+0.37}_{-0.37}$	$25.9^{+3.7}_{-3.7}$ [10] $9.7^{+1.1}_{-1.1}$ [11] $27.0^{+3.9}_{-3.9}$ [18]	$19.15^{+0.50}_{-0.50}$	$29.0^{+2.8}_{-2.8}$ [10]	$23.52^{+0.76}_{-0.76}$	–	–	–	–	–

Notes. Average pitch angle measurements of the spiral arms (from northern and southern pitch angles) in degrees from the SPIRALITY for different wavebands as shown in the table. Existing values obtained from the literature are indicated with references.

References. [1] (Davis 2015b). [2] (Martínez-García 2012). [3] (Ma 2001). [4] (Seigar et al. 2006). [5] (Berrier et al. 2013). [6] (Pan 2021). [7] (Hewitt & Treuthardt 2020). [8] (Al-Baidhany et al. 2019). [9] (Díaz-García et al. 2019). [10] (Abdeen 2021). [11] (Yu & Ho 2018). [12] (Miller et al. 2019). [13] (Kennicutt 1981). [14] (Puerari & Dottori 1992). [15] (Ma, Peng & Gu 1998). [16] (Danver 1942). [17] (Considere & Athanassoula 1982). [18] (Abdeen et al. 2020).

pitch angle, in degrees, for both arms of $31.5^{+1.6}_{-3.2}$ using a Fourier method. There are two main reasons for this sharp disagreement of pitch angles. (a) Martínez-García (2012) has considered a radial range (innermost radius to outermost radius) of 56.1–95.8 arcsec for this pitch angle measurement. (b) NGC 7479 is a barred spiral galaxy, and in general, the spiral arms of this object clearly deviate from being logarithmic. Thus, measuring an average pitch angle using the Fourier method would give a higher pitch angle value than expected.

Upon closer examination of the pitch angle measurements, it is evident that the strongest correlations are observed in the Hα (Fig. 4d) and 3.6 μm (Fig. 4b) bands. The pitch angle measurements for the Hα and 3.6 μm bands with literature values show less scatter compared to other bands, indicating a more robust agreement. This can be attributed to the fact that Hα emission predominantly traces regions of active star formation, which are closely associated with the spiral density waves. Similarly, the 3.6 μm band is sensitive to the old stellar population, which forms the backbone of the spiral arms and is less affected by dust extinction, leading to more precise measurements. These findings suggest that Hα and 3.6 μm bands serve as the most consistent tracers for spiral arm pitch angles, providing reliable data less susceptible to variations caused by observational biases or environmental factors.

4.3 Pitch angle correlations with 8.0 μm waveband

The average pitch angles of the spiral arms (calculated from the northern and southern pitch angles) measured in the 8.0 μm band were compared with the average pitch angles measured in the B

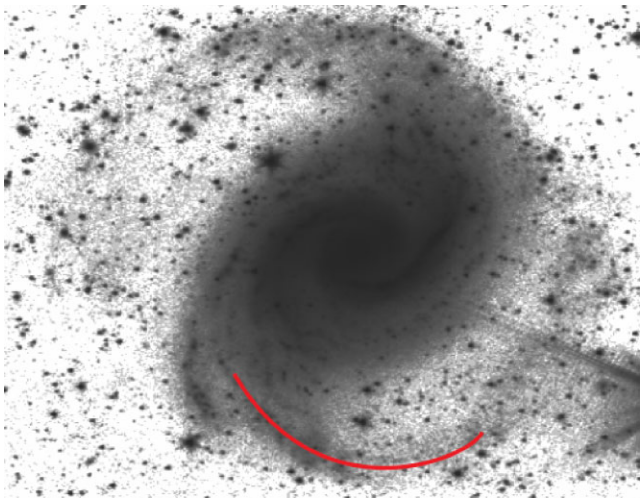

Figure 1. The pitch angles of one of the outer arms of NGC 1566 were measured considering the arm segment, as indicated by the solid red line. This is depicted using the 3.6 μm image of NGC 1566 as an example. Image source: NASA/IPAC Extragalactic Database (NED)[5].

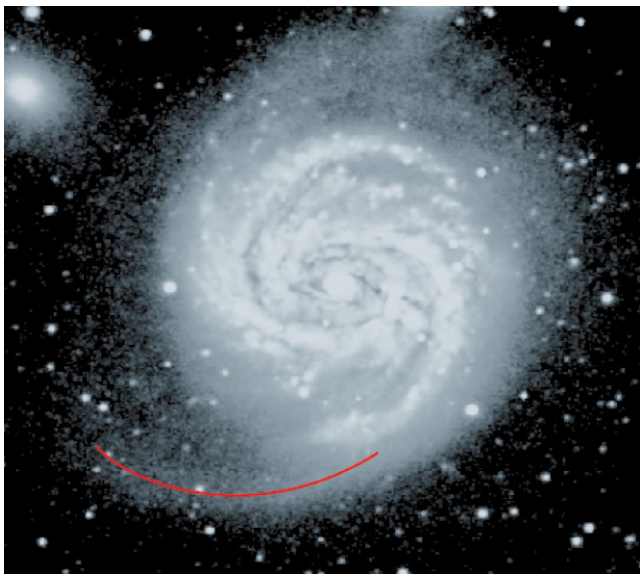

Figure 2. The pitch angles of the southern outer arm of NGC 4321 were measured considering the arm segment, as indicated by the solid red line. This image was generated by converting an optical image to a FITS format.

band, 3.6 μm, and H α bands based on the availability of data (CO and H I bands were excluded due to lack of data) (see Fig. 5). In this study, we measured the average pitch angles of the spiral arms by considering the entire visible extent of the spiral arms in the images corresponding to each waveband (*B* band, 3.6 μm, 8 μm, and H α). Our methodology did not confine the measurements to a specific radius, but instead encompassed the full length of the spiral arms as they appear in the respective waveband images. This approach allows for a comprehensive assessment of the spiral structure, capturing the overall morphology and providing a more accurate representation of the pitch angles across the different wavelengths. By including the entire visible extent of the spiral arms, we ensure that our measurements reflect the true nature of the galactic spiral structure,

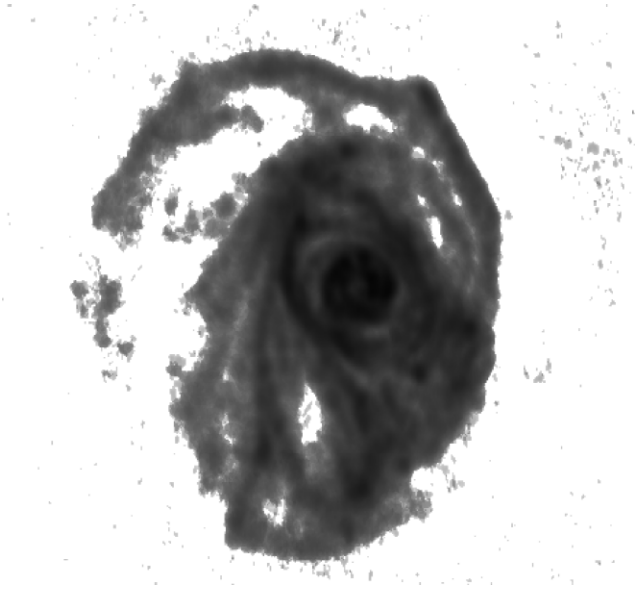

Figure 3. H I outer arm of NGC 5236. Image source: The Local Volume HI Survey (LVHIS) (Koribalski et al.2018).

free from biases introduced by radial limitations. The dashed line represents the 1:1 relationship ($y = x$) in each panel, and the best-fitting straight line, whose functional form is given at the top, is marked by the solid blue line. It is apparent that the 3.6 and 8.0 μm images give identical pitch angles for the spiral arms. This provides a theoretical evidence for the experimental observation that old stars typically conglomerate near the dust lanes. A previous study by Seigar et al. (2006) found a nearly 1:1 correlation between pitch angle measurements in the *B* and H bands for 57 galaxies in the OSUBGS (Eskridge et al. 2002) sample.

4.4 Black hole mass calculations

In this study, we employed equation (2) from Berrier et al. (2013) to estimate the SMBH masses. The equation was derived using the directly measured black hole masses based on stellar and gas dynamics, masers, and reverberation mapping techniques.

$$\log\left(\frac{M_{\rm BH}}{\rm M_{\odot}}\right) = (8.21 \pm 0.16) - (0.062 \pm 0.009)P, \quad (2)$$

where $M_{\rm BH}$ is the black hole mass, $\rm M_{\odot}$ is the solar mass, and P stands for the pitch angle of the galaxy in degrees. When using equation (2) to calculate black hole masses, it is important to consider the limitations mentioned in the introduction of this paper, as well as specific limitations associated with the equation. First, the sample used to derive this equation is primarily based on galaxies with relatively large SMBH masses and tightly wound spiral arms (pitch angles $P < 15^{\circ}$), leading to a lack of data for galaxies with more loosely wound spirals. This selection bias can affect the general applicability of the equation across different types of spiral galaxies. Secondly, measurement errors in pitch angles, particularly in poor-quality data or flocculant galaxies, can significantly impact the accuracy of the estimated black hole masses. Additionally, the SMBH masses in the sample were derived using various methods, including stellar/gas dynamics, maser modelling, and reverberation mapping, each with its own assumptions and potential biases, resulting in variations and inconsistencies. The intrinsic scatter in this SMBH

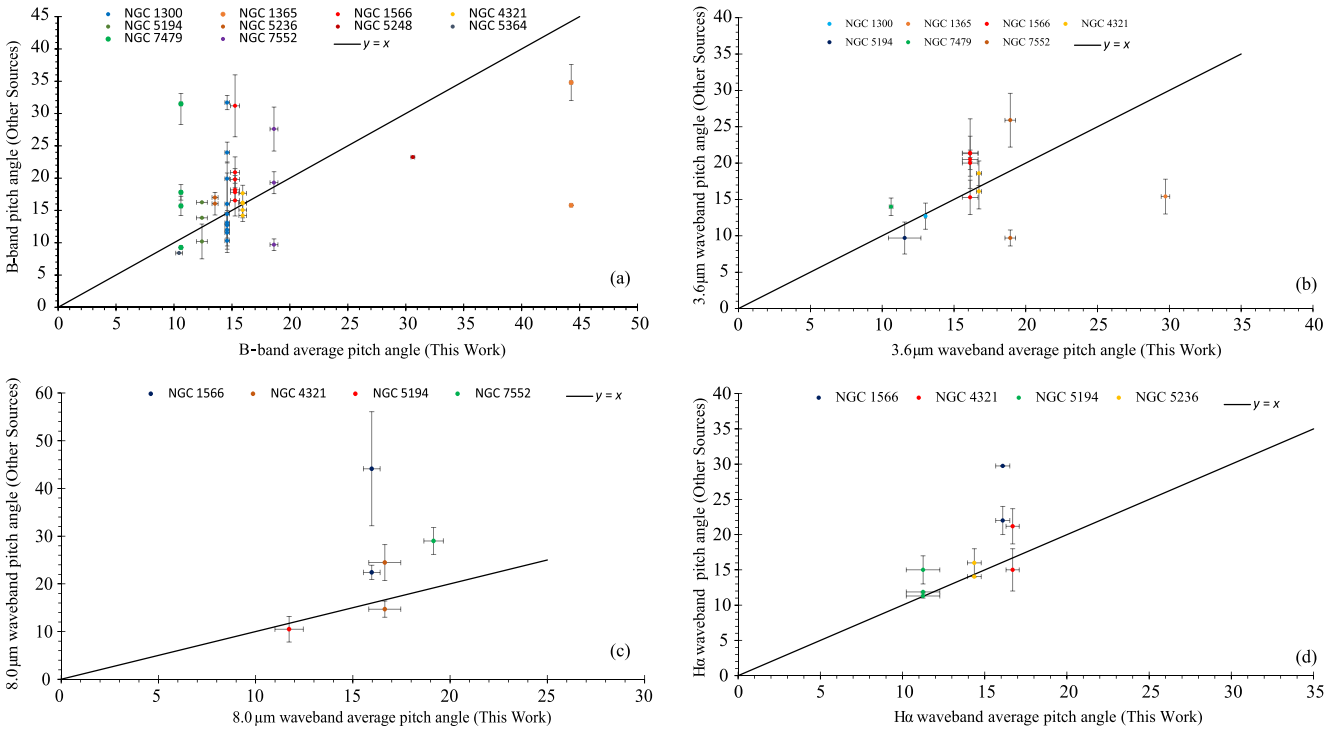

Figure 4. (a): comparison of *B*-band pitch angles (other sources) with *B*-band average pitch angles (this work). (b): comparison of 3.6 μm waveband pitch angles (other sources) with 3.6 μm average pitch angles (this work). (c): comparison of 8.0 μm waveband pitch angles (other sources) with 8.0 μm average pitch angles (this work). (d): comparison of H α waveband pitch angles (other sources) with Hα average pitch angles (this work). Black solid line: one-to-one relation.

mass–pitch angle relation, which is 0.38 dex, indicates a significant level of inherent uncertainty (Berrier et al. 2013).

The underlying density wave is believed to be well represented by the 3.6 μm waveband. In addition, this waveband represents the old stellar population. Thus, we used the pitch angles of 3.6 μm waveband to calculate black hole masses. On the contrary, we could not measure the pitch angles of the outer arms of NGC 4321, NGC 5236, and NGC 5248 using images corresponding to 3.6 μm waveband. We used some alternative methods to estimate the rough pitch angle values of these outer arms (see Section 4.1), and these pitch angles were used to calculate black hole masses when applicable. As discussed, our galaxy sample can be categorized into two groups: one group includes galaxies with inner arms only, while the other group includes both inner and outer arms. We calculated black hole masses for galaxies with both inner and outer arms using the pitch angles of the inner arms and outer arms separately. The calculated SMBH masses of galaxies are shown in Tables 4 (galaxies with inner arms only) and 5 (galaxies with both inner and outer arms).

4.5 Comparison of black hole masses

Fig. 6 (a) shows the comparison of our black hole masses with values in the literature. The average pitch angles of the 3.6 μm waveband were used to determine the black hole masses. For the five galaxies with both inner and outer arm structures, we have included average black hole masses calculated using two black hole masses determined by the average pitch angles of the inner and outer arms (see Table 5). The graph indicates a significant deviation with considerable discrepancies between our black hole masses and the values in the literature. Thus, it manifests that these 10 galaxies should be studied separately by categorizing them into two groups, namely galaxies with inner arms and galaxies with both inner and outer arms.

Fig. 6(b) shows the comparison of our calculated black hole masses with the black hole masses found in the literature for galaxies with inner arms. Our calculations are nearly comparable to the literature value when these five galaxies are studied separately.

Fig. 7 shows a comparison of our black hole masses with the literature value for galaxies with both inner and outer arms. Black hole masses were determined using the average pitch angles of the outer and inner arms by the 3.6 μm waveband (see Table 5). Black hole masses determined by the average pitch angles of the inner arms are shown to be more comparable to those found in the literature (see Fig. 7b). According to our data sample, we conclude that the black hole mass of a galaxy with both inner arms and outer arms is governed by the average pitch angle of the inner arms. Consequently, this implies that there is a strong relationship between the black hole mass and the inner arms of the spiral galaxy.

4.6 The M_{BH}–P relation

As shown in Fig. 8(a), we plotted black hole masses found in the literature against our 3.6 μm waveband average pitch angle measurements of galaxies with inner arms. We found a linear fit of the form

$$\log\left(\frac{M_{\rm BH}}{\rm M_{\odot}}\right) = (7.11 \pm 0.33) + (0.003 \pm 0.017)P, \quad (3)$$

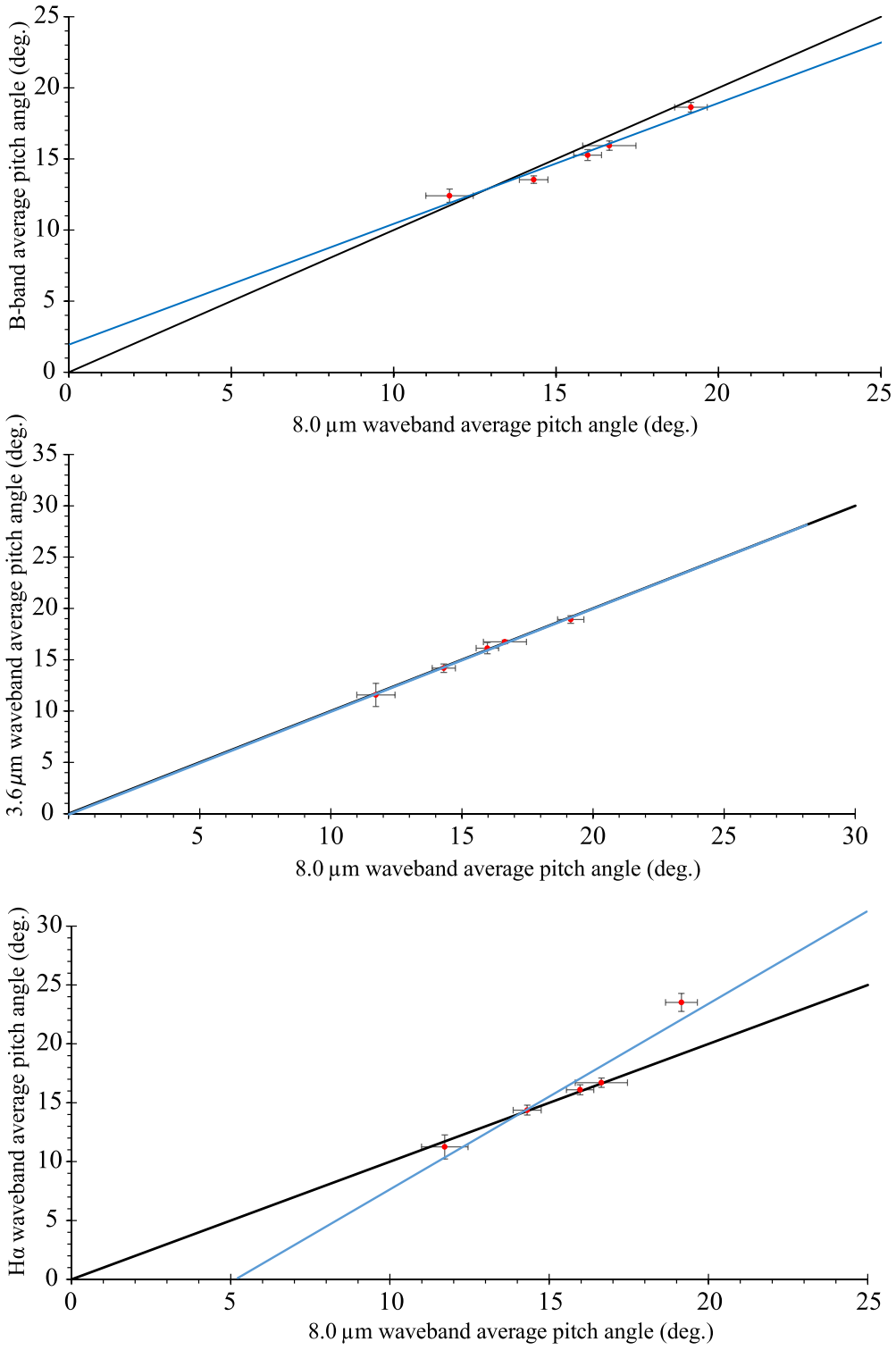

Figure 5. Correlations between the average pitch angle of the spiral arms in the 8.0 μm band and in the *B* (top graph), 3.6 μm (middle graph), and H α (bottom graph) bands. Black solid line: one-to-one relation; solid blue line: best-fitting line.

where $M_{\rm BH}$ is the black hole mass, $M_\odot$ is the solar mass, and P stands for the pitch angle of the galaxy in degrees. We propose that the SMBH mass–pitch angle relation (3) is ideal for measuring the SMBH mass of galaxies with only inner arms.

Fig. 8(b) shows the graph of black hole masses found in the literature against 3.6 μm waveband average pitch angles measurements of the inner arms of galaxies with both inner and outer arms (based on the conclusion in Section 4.5). We found an SMBH mass–pitch angle relation of

$$\log\left(\frac{M_{\rm BH}}{M_\odot}\right) = (7.56 \pm 0.28) - (0.038 \pm 0.013)P, \quad (4)$$

Table 4. Black hole mass calculations for galaxies with inner arms using 3.6 μm waveband pitch angles.

galaxy	log (M_{BH}/M$_\odot$)			Existing values
	By northern pitch angle	By southern pitch angle	By average pitch angle	
(1)	(2)	(3)	(4)	(5)
NGC 1300	7.627 ± 0.181	7.180 ± 0.219	7.403 ± 0.198	7.42 ± 0.23 (B band) [1]
				7.82 ± 0.29 [2]
				7.83 ± 0.29 [a] [3]
				$7.86^{+0.29}_{-0.28}$ [a] [4]
				7.568 ± 0.17 [5]
				$7.85^{+0.47}_{-0.31}$ [a] [6] [7]
				7.88 ± 0.34 [a] [8] [9]
				7.85 ± 0.29 [a] [10]
				$7.71^{+0.17}_{-0.12}$ [a] [11]
				$7.71^{+0.19}_{-0.14}$ [a] [12] [13]
				7.878 ± 0.343 [a] [14]
NGC 1365	6.525 ± 0.293	6.209 ± 0.333	6.367 ± 0.312	6.30 ± 0.4 [15]
				7.84 ± 0.26 [16]
				6.60 ± 0.3 [a] [16]
				6.05 ± 0.39 [1]
				7.639 ± 0.07 [5]
				7.3 ± 0.4 (0.3) [15]
				7.8 ± 0.4 (0.3) [15]
				7.66 [17] [18]
NGC 5194	7.498 ± 0.198	7.488 ± 0.231	7.493 ± 0.203	6.95 [19] [20] [21]
				6.32/5.60 [a] [7]
				$5.96^{+0.36}_{-5.96}$ [a] [8] [9]
				6.38/5.66 [a] [22]
				6.85 [23]
				6.9 [17]
NGC 7479	–	7.552 ± 0.187	7.552 ± 0.187	7.07 [20] [24]
				7.7 [25]
NGC 7552	7.037 ± 0.235	–	7.037 ± 0.235	7.28 ± 0.33 [1]
				6.9 [25]

Notes. Columns: (1) galaxy name. (2) Black hole mass derived from northern spiral arm pitch angle. (3) Black hole mass derived from southern spiral arm pitch angle. (4) Black hole mass derived from average pitch angle. (5) Existing values obtained from literature with references (All literature values have been converted to logarithmic scale (Log10) for ease of comparison).
References. [1] (Davis et al. 2014). [2] (Atkinson et al. 2005). [3] (Graham 2008). [4] (Graham & Scott 2013). [5] (Al-Baidhany et al. 2019). [6] (Gültekin et al. 2009). [7] (Beifiori et al. 2012). [8] (van den Bosch 2016). [9] (Dullo et al. 2020). [10] (Berrier et al. 2013). [11] (Davis, Graham & Seigar 2017). [12] (Davis, Graham & Cameron 2019a). [13] (Davis, Graham & Combes 2019b). [14] (Saglia et al. 2016). [15] (Risaliti et al. 2009). [16] (Combes et al. 2019). [17] (Merloni, Heinz & Di Matteo 2003). [18] (Simien & Prugniel 2002) [19] (Woo & Urry 2002). [20] (Panessa et al. 2006). [21] (Ter-Kazarian 2015). [22] (Pagotto 2018). [23] (İkiz et al. 2020). [24] (Wang, Zhang & Fan 2010). [25] (Cisternas et al. 2013).
[a] Direct black hole mass measurement (especially from stellar or gas kinematics).

where $M_{\rm BH}$ is the black hole mass, M$_\odot$ is the solar mass, and P stands for the pitch angle of the galaxy in degrees. We recommend equation (4) to measure the SMBH mass of galaxies with both inner arms and outer arms.

5 SUMMARY AND CONCLUSIONS

This research primarily focuses on testing predictions of density wave theory using multiwavelength image data. The cardinal objective of the study is to verify the wavelength dependence of the pitch angles using image analysis. Upon measuring the pitch angles we aimed to determine black hole masses using a scaling relation found in the literature. Our galaxy sample consisted of two types of galaxies: galaxies with inner arms and galaxies with both inner and outer arms. The pitch angles were initially measured using the PYTHON-OLSCRIPT with more precise and reliable measurements obtained using the SPIRALITY Matlab script. The pitch angles were measured for each spiral arm separately. We graphically interpreted the effectiveness of measuring the pitch angles for each arm separately instead of measuring an average pitch angle. By analysing pitch angles in the B band, 3.6 μm, 8.0 μm, Hα, CO, and H I, we demonstrated the dependence of pitch angles on wavelengths. In this work, we have included CO and H I waveband pitch angle measurements that were not previously reported in the literature. Furthermore, we were able to find a 1:1 correlation between pitch angle measurements in the 3.6 and 8.0 μm bands.

Table 5. Black hole mass calculations for galaxies with both inner and outer arms using 3.6 μm waveband pitch angles.

galaxy	log (M_{BH}/$M_\odot$)						Existing values
	Inner arms			Outer arms			
	Northern	Southern	Average	Northern	Southern	Average	
(1)	(2)	(3)	(4)	(5)	(6)	(7)	(8)
NGC 1566	6.785 ± 0.262	6.902 ± 0.251	6.843 ± 0.256	7.148 ± 0.232	7.273 ± 0.210	7.210 ± 0.219	6.83 ± 0.3^a [1]
							7.13 ± 0.10 [1]
							6.70^a [2] [3]
							6.92 [4]
							$6.93^{+0.18}_{-0.31}$ [5]
							6.78 (upper limit) [5]
							$6.62^{+0.2}_{-0.37}$ [5]
							$6.72^{+0.19}_{-0.34}$ (Mean) [5]
							6.919 ± 0.07 [6]
							6.48 ± 0.2 [5]
							7.11 ± 0.32 [7]
NGC 4321	7.367 ± 0.202	6.977 ± 0.241	7.172 ± 0.220	–	6.555 ± 0.311	6.555 ± 0.311	6.8 [8] [9]
							7.43/7.40 (Upper)^a [10]
							6.36 (sensitivity limit)^a [10]
							6.36 [11]
							$7.345^{+0.136}_{-0.150}$ [12]
							$7.26/6.56^a$ [13]
							$6.84/6.51^a$ [14]
							$6.67^{+0.17}_{-6.67}{}^a$ [15]
NGC 5236	7.331 ± 0.205	7.331 ± 0.210	7.331 ± 0.206	–	7.658 ± 0.179	7.658 ± 0.179	7.22 ± 0.24 [7]
NGC 5248	6.670 ± 0.276	5.963 ± 0.365	6.317 ± 0.319	7.491 ± 0.191	7.509 ± 0.190	7.499 ± 0.190	$6.85/6.11^a$ [13]
							$6.30^{+0.38}_{-0.38}{}^a$ [16]
							$6.68/5.92^a$ [14]
NGC 5364	6.917 ± 0.248	6.640 ± 0.279	6.778 ± 0.263	7.536 ± 0.189	7.570 ± 0.193	7.553 ± 0.189	6.12 ± 0.15^b

Notes. Columns: (1) galaxy name. (2) Black hole mass derived from northern inner spiral arm pitch angle. (3) Black hole mass derived from southern inner spiral arm pitch angle. (4) Black hole mass derived from average pitch angle of inner arms. (5) Black hole mass derived from northern outer spiral arm pitch angle. (6) Black hole mass derived from southern outer spiral arm pitch angle. (7) Black hole mass derived from average pitch angle of outer arms. (8) Existing values obtained from literature with references (Some of the literature values have been converted to logarithmic scale (Log10) for ease of comparison).
References. [1] (Combes et al. 2019). [2] (Kriss et al. 1991). [3] (Alloin et al. 1986). [4] (Woo & Urry 2002). [5] (Smajić et al. 2015). [6] (Al-Baidhany et al. 2019). [7] (Davis et al. 2014). [8] (Merloni et al. 2003). [9] (Barth, Ho & Sargent 2002). [10] (Sarzi et al. 2002). [11] (Satyapal et al. 2008). [12] (Berrier et al. 2013). [13] (Pagotto 2018). [14] (Beifiori et al. 2012). [15] (van den Bosch 2016). [16] (Dullo et al. 2020).
[a] Direct black hole mass measurement (especially from stellar or gas kinematics).
[b] Calculated through M-σ equation from Tundo et al. (2007) and $\sigma = 57.08$ km s^{-1} (Alam et al. 2015).

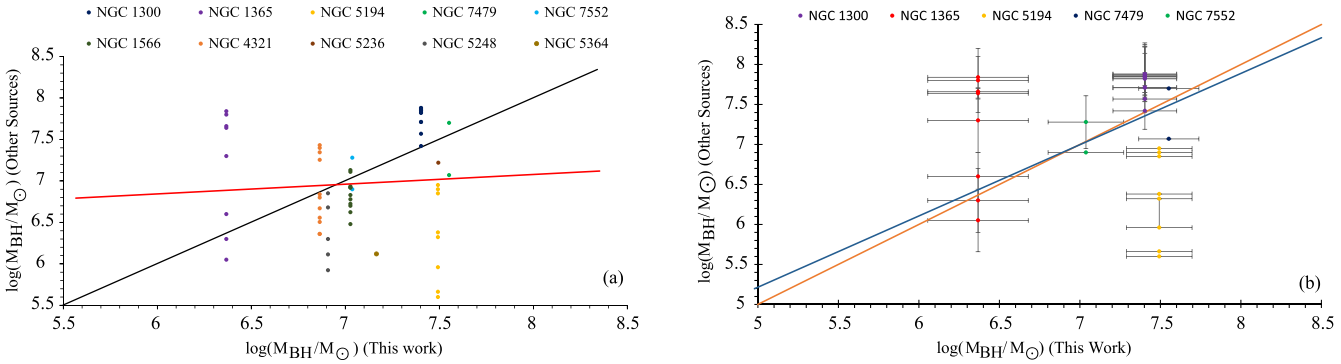

Figure 6. (a): black hole mass (other sources) versus black hole mass calculated by the 3.6 μm waveband average pitch angle (this work); data shown in Tables 4 and 5. Black solid line: one-to-one relation; red-solid line: best-fitting straight line. (b): black hole mass (other sources) versus black hole mass calculated by the 3.6 μm waveband average pitch angle (this work) of galaxies with inner arms; data shown in Table 4. Orange-solid line: one-to-one relation; blue-solid line: best-fitting straight line.

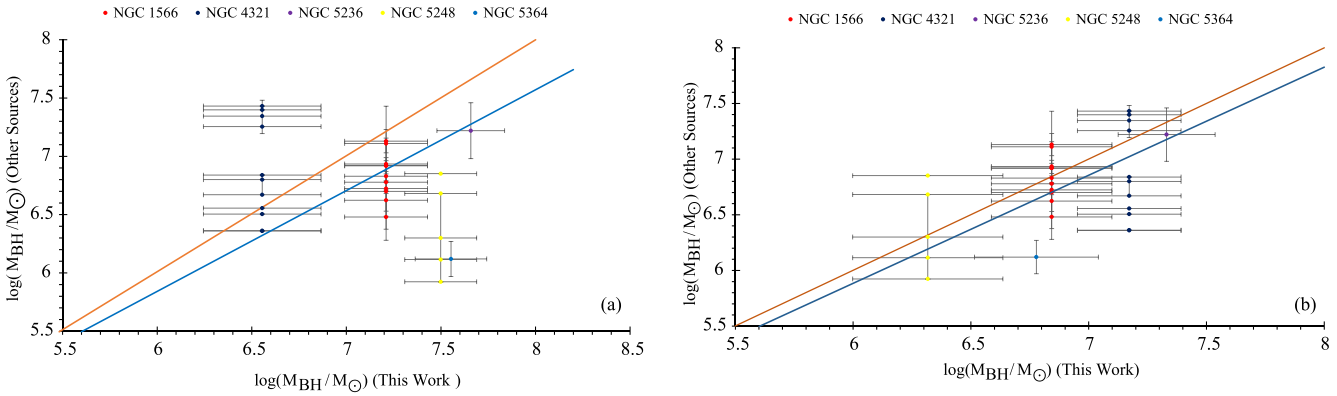

Figure 7. (a): black hole mass (other sources) versus black hole mass calculated by the 3.6 μm waveband average pitch angle of the outer arms (this work) of galaxies with both inner and outer arms; data shown in Table 5. (b): black hole mass (other sources) versus black hole mass calculated by the 3.6 μm waveband average pitch angle of the inner arms (this work) of galaxies with both inner and outer arms; data shown in Table 5. Orange-solid line: one-to-one relation; blue-solid line: best-fitting line.

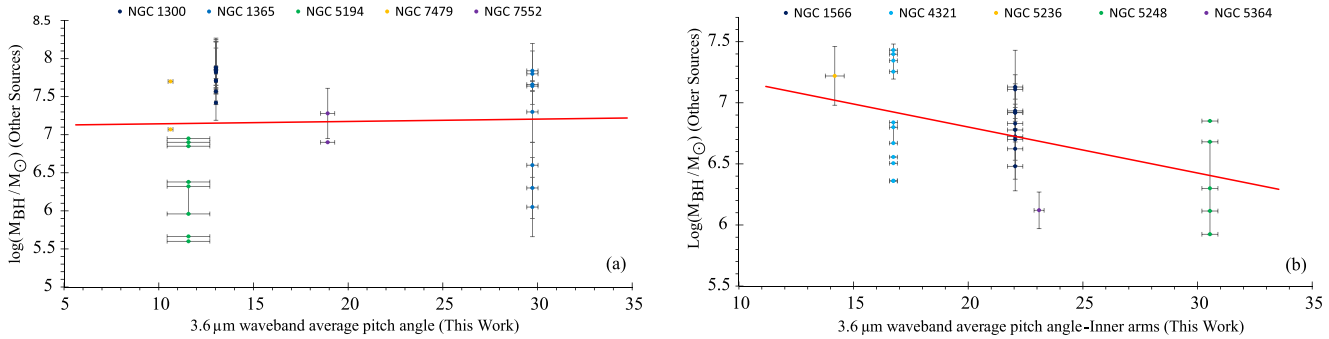

Figure 8. (a): black hole mass (other sources) versus 3.6 μm waveband average pitch angle (this work) of galaxies with inner arms. (b): black hole mass (other sources) versus 3.6 μm waveband average pitch angle of the inner arms (this work) of galaxies with both inner arms and outer arms. Red-solid line: best-fitting line.

We obtained black hole masses using equation (2) with pitch angle measurements of the 3.6 μm waveband. Most of the black hole masses of galaxies with inner arms were comparable to the values in the literature. We calculated the black hole masses of galaxies with both inner and outer arms by measuring the pitch angles of the inner and outer arms separately. Based on our data sample, we demonstrated that the black hole mass of a galaxy with both inner and outer arms is determined by the average pitch angle of the inner arms. For galaxies with only inner arms, we found an SMBH mass–pitch angle relation of

$$\log\left(\frac{M_{\rm BH}}{\rm M_\odot}\right) = (7.11 \pm 0.33) + (0.003 \pm 0.017)P.$$

Besides, for galaxies with both inner and outer arms, we found a linear fit of the form

$$\log\left(\frac{M_{\rm BH}}{\rm M_\odot}\right) = (7.56 \pm 0.28) - (0.038 \pm 0.013)P.$$

ACKNOWLEDGEMENTS

The authors gratefully acknowledge Douglas W. Shields for writing the original SPIRALITY code, which was used to measure ideal galactic spiral arm pitch angles. This research has used the NASA/IPAC Extragalactic Database (NED), The Local Volume HI Survey (LVHIS), and the NASA's Astrophysics Data System.

DATA AVAILABILITY

The data underlying this article will be shared on reasonable request to the corresponding author.

REFERENCES

Abdeen M. S., 2021, Testing Spiral Density-Wave Theory in Disk Galaxies Using Multi-Wavelength Image Data, Star Formation History Maps and Spatially Resolved Stellar Clusters. University of Arkansas, Arkansas, USA
Abdeen S., Kennefick D., Kennefick J., Miller R., Shields D. W., Monson E. B., Davis B. L., 2020, MNRAS, 496, 1610
Al-Baidhany I. A., et al., 2019, IOP Conf. Ser.: Mater. Sci. Eng., 571, 012118
Alam S. et al., 2015, ApJS, 219, 12
Alloin D., Pelat D., Phillips M. M., Fosbury R. A. E., Freeman K., 1986, ApJ, 308, 23
Athanassoula E., 2012, MNRAS, 426, L46
Atkinson J. W. et al., 2005, MNRAS, 359, 504
Barth A. J., 2003, preprint(arxiv:astro-ph/0310436)
Barth A. J., Ho L. C., Sargent W. L. W., 2002, AJ, 124, 2607
Beck R., 2016, A&AR, 24, 4
Beifiori A., Courteau S., Corsini E. M., Zhu Y., 2012, MNRAS, 419, 2497

Berrier J. C. et al., 2013, ApJ, 769, 132
Bertin G., 2014, in Dynamics of Galaxies, Spiral Structure in Galaxies. Cambridge University Press, Cambridge, p.247
Bertin G., 1993, PASP, 105, 640
Bertin G., Lin C. C., Lowe S. A., Thurstans R. P., 1989a, ApJ, 338, 78
Bertin G., Lin C.-C., 1996, Spiral Structure in Galaxies: A Density Wave Theory. MIT Press, Cambridge, MA
Bertin G., Lin C., Lowe S., Thurstans R., 1989b, ApJ, 338, 104
Block D. L., Puerari I., Frogel J. A., Eskridge P. B., Stockton A., Fuchs B., 1999, Ap&SS, 269, 5
Chemin L. et al., 2006, MNRAS, 366, 812
Cisternas M. et al., 2013, ApJ, 776, 50
Combes F. et al., 2019, A&A, 623, A79
Considere S., Athanassoula E., 1982, A&A, 111, 28
Danver C.-G., 1942, Annals of the Observatory of Lund, 10, 3
Davis B. L. et al., 2014, ApJ, 789, 124
Davis B. L. et al., 2015, ApJ, 802, L13
Davis B. L., Graham A. W., Cameron E., 2019a, ApJ, 873, 85
Davis B. L., Graham A. W., Combes F., 2019b, ApJ, 877, 64
Davis B. L., Graham A. W., Seigar M. S., 2017, MNRAS, 471, 2187
Davis B., 2015a, Logarithmic Spiral Arm Pitch Angle of Spiral Galaxies: Measurement and Relationship to Galactic Structure and Nuclear Supermassive Black Hole Mass. University of Arkansas, Arkansas, USA
Davis B., 2015b, PhD thesis, Univ. Arkansas
Díaz-García S., Salo H., Knapen J. H., Herrera-Endoqui M., 2019, A&A, 631, A94
Dobbs C., Baba J., 2014, Publ. Astron. Soc. Aust., 31, e035
Dullo B. T., Bouquin A. Y. K., de Paz A. G., Knapen J. H., Gorgas J., 2020, ApJ, 898, 83
Elmegreen B. G., Elmegreen D. M., 1985, ApJ, 288, 438
Elmegreen D. M. et al., 2011, ApJ, 737, 32
Elmegreen D. M., 1998, Galaxies and Galactic Structure. Prentice Hall, Upper Saddle River, NJ
Elmegreen D. M., Elmegreen B. G., 1987, ApJ, 314, 3
Eskridge P. B. et al., 2002, ApJS, 143, 73
Evans A. S. et al., 2022, ApJ, 940, L8
Font J., Beckman J. E., James P. A., Patsis P. A., 2019, MNRAS, 482, 5362
Fuchs B., Sundelius B., 1991, in Dynamics of Disc galaxies, Dept. Astron. Astrophys., Chalmers Univ. of Technology, Göteborg, Sweden, p. 359
Fuchs B., 2000, in Combes F., Mamon G. A., Charmandaris V., eds, ASP Conf. Ser. Vol. 197, Dynamics of Galaxies: from the Early Universe to the Present. Astron. Soc. Pac., San Francisco, p. 53
García-Burillo S. et al., 2003, A&A, 407, 485
Gardner J. P. et al., 2023, PASP, 135, 068001
Genel S. et al., 2014, MNRAS, 445, 175
Gnedin O. Y., Goodman J., Frei Z., 1995, AJ, 110, 1105
Graham A. W., 2008, ApJ, 680, 143
Graham A. W., Scott N., 2013, ApJ, 764, 151
Graham A. W., Worley C. C., 2008, MNRAS, 388, 1708
Grand R. J., Kawata D., Cropper M., 2013, A&A, 553, A77
Grosbøl P., Patsis P. A., Pompei E., 2004, A&A, 423, 849
Gültekin K. et al., 2009, ApJ, 698, 198
Hensley K., 2023, AAS Nova Highlights, p. 10776
Herrera-Endoqui M., Díaz-García S., Laurikainen E., Salo H., 2015, A&A, 582, A86
Hewitt I. B., Treuthardt P., 2020, MNRAS, 493, 3854
Huchtmeier W. K., Bohnenstengel H.-D., 1981, A&A, 100, 72
İkiz T., Peletier R. F., Barthel P. D., Yeşilyaprak C., 2020, A&A, 640, A68
Jarrett T. et al., 2012, AJ, 145, 6
Kendall S., Clarke C., Kennicutt Jr R., 2015, MNRAS, 446, 4155
Kennicutt R. C. Jr, 1981, AJ, 86, 1847
Koribalski B. S. et al., 2018, MNRAS, 478, 1611
Kormendy J., 2004, in Ho L. C.ed., Coevolution of Black Holes and Galaxies. Cambridge Univ. Press, Cambridge, p. 1
Kormendy J., Kennicutt Jr R. C., 2004, ARA&A, 42, 603
Kormendy J., Richstone D., 1995, ARA&A, 33, 581
Kriss G. A., Hartig G. F., Armus L., Blair W. P., Caganoff S., Dressel L., 1991, ApJ, 377, L13
Lee J. C. et al., 2023, ApJ, 944, L17
Lin C. C., Shu F. H., 1964, ApJ, 140, 646
Lin C., Shu F. H., 1966, Proc. Natl. Acad. Sci., 55, 229
Lin C., Shu F. H., 1987, Selected Papers of CC Lin with Commentary: Vol. 1: Fluid Mechanics Vol. 2: Astrophysics. World Scientific, Singapore, p.561
Lindblad B., 1940, ApJ, 92, 1
Lindblad B., 1942, Stockholms Observatoriums Annaler, 14, 1.1
Lindblad B., 1948, Stockholms Observatoriums Annaler, 15, 4.1
Lindblad B., 1950, Stockholms Observatoriums Annaler, 0016, 1.1
Lindblad B., 1955, Stockholms Observatoriums Annaler, 6, 6
Lindblad B., 1957, Differential Motions in Dispersion Orbits in the Galaxy, Etc. Almqvist and Wiksell, Stockholm, Sweden
Lindblad B., 1958a, Stockholms Observatoriums Annaler, 4, 4
Lindblad B., 1958b, Stockholms Observatoriums Annaler, 6, 6
Lindblad B., 1961, Stockholms Observatoriums Annaler, 8, 8
Lindblad B., 1963, Stockholms Observatoriums Annaler, 5, 5
Lindblad B., 1964, Astrophys. Nor., 9, 103
Lindblad B., Langebartel R. G., 1953, Stockholms Observatoriums Annaler, 17, 6
Lindblad B., Langebartel R., 1956, Stockholms Observatoriums Annaler. Almquist & Wiksell, Stockholm, Sweden
Ma J., 2001, Chinese J. Astron. Astrophys., 1, 395
Ma J., Peng Q.-H., Gu Q.-S., 1998, A&AS, 130, 449
Magorrian J. et al., 1998, AJ, 115, 2285
Martínez-García E. E., 2011, ApJ, 744, 92
Martínez-García E. E., 2012, ApJ, 744, 92
McElwain M. W. et al., 2023, PASP, 135, 058001
Menzel M. et al., 2023, PASP, 135, 058002
Merloni A., Heinz S., Di Matteo T., 2003, MNRAS, 345, 1057
Michikoshi S., Kokubo E., 2014, ApJ, 787, 174
Miller R., Kennefick D., Kennefick J., Abdeen M. S., Monson E., Eufrasio R. T., Shields D. W., Davis B. L., 2019, ApJ, 874, 177
Muñoz-Mateos J. C. et al., 2015, ApJS, 219, 3
Mutlu-Pakdil B., Seigar M. S., Hewitt I. B., Treuthardt P., Berrier J. C., Koval L. E., 2018, MNRAS, 474, 2594
Pagotto I., 2018, Mass determination of supermassive black holes in nearby galaxies. University of Padua, Padua (Padova), Italy
Pan H., 2021, Int. J. Phys., 9, 71
Panessa F., Bassani L., Cappi M., Dadina M., Barcons X., Carrera F. J., Ho L. C., Iwasawa K., 2006, A&A, 455, 173
Peltonen J. et al., 2024, MNRAS, 527, 10668
Pour-Imani H., 2018, Strong Evidence for the Density-wave Theory of Spiral Structure from a Multi-wavelength Study of Disk Galaxies. University of Arkansas, Arkansas, USA
Puerari I., Dottori H. A., 1992, A&AS, 93, 469
Purcell C. W., Bullock J. S., Tollerud E. J., Rocha M., Chakrabarti S., 2011, Nature, 477, 301
Ringermacher H. I., Mead L. R., 2009, MNRAS, 397, 164
Risaliti G. et al., 2009, ApJ, 696, 160
Roberts Jr W. W., 1975, Vistas Astron., 19, 91
Roberts W. W. Jr, Roberts M. S., Shu F. H., 1975, ApJ, 196, 381
Rohlfs K., 1977, Lectures on Density Wave Theory. Lecture Notes in Physics, Vol. 69, Springer-Verlag, Berlin
Saglia R. P. et al., 2016, ApJ, 818, 47
Sandage A., 1961, The Hubble Atlas of Galaxies. Carnegie Institution, Washington
Sandstrom K. M. et al., 2023, ApJ, 944, L8
Sarzi M. et al., 2002, ApJ, 567, 237
Satyapal S., Vega D., Dudik R. P., Abel N. P., Heckman T., 2008, ApJ, 677, 926
Savchenko S. S., Reshetnikov V. P., 2013, MNRAS, 436, 1074
Schweizer F., 1976, ApJS, 31, 313
Seigar M. S., 2017, Spiral Structure in Galaxies. Morgan and Claypool Publishers, San Rafael, California.
Seigar M. S., Block D., Puerari I., 2004, in Block D. L., Puerari I., Freeman K. C., Groess R., Block E. K., eds, Astrophysics and Space Science Library,

Vol. 319, Penetrating Bars Through Masks of Cosmic Dust: The Hubble Tuning Fork Strikes a New Note. Springer-Verlag, Berlin, p. 155
Seigar M. S., Block D., Puerari I., Chorney N., James P., 2005, MNRAS, 359, 1065
Seigar M. S., Bullock J. S., Barth A. J., Ho L. C., 2006, ApJ, 645, 1012
Seigar M. S., Davis B. L., Berrier J., Kennefick D., 2014, ApJ, 795, 90
Seigar M. S., Kennefick D., Kennefick J., Lacy C. H. S., 2008, ApJ, 678, L93
Shetty R., Vogel S. N., Ostriker E. C., Teuben P. J., 2007, ApJ, 665, 1138
Shields D. et al., 2022, Galaxies, 10, 100
Shields D. W., Boe B., Henderson C. L., Hartley M., Davis B. L., Pour Imani H., Kennefick D., Kennefick J. D., 2015, in American Astronomical Society Meeting Abstracts #225. American Astronomical Society,Washington, D.C. p. 250.09
Shu F. H., 2016, ARA&A, 54, 667
Simien F., Prugniel P., 2002, A&A, 384, 371
Smajić S., Moser L., Eckart A., Busch G., Combes F., García-Burillo S., Valencia-S. M., Horrobin M., 2015, A&A, 583, A104
Ter-Kazarian G., 2015, Journal of Astrophysics, 173, 30
Thilker D. A. et al., 2007, ApJS, 173, 538
Tundo E., Bernardi M., Hyde J. B., Sheth R. K., Pizzella A., 2007, ApJ, 663, 53
van den Bosch R. C. E., 2016, ApJ, 831, 134
Visser H. C. D., 1980, A&A, 88, 149
Wang J., Zhang J.-S., Fan J.-H., 2010, Res. Astron. Astrophys., 10, 915
Whitmore B. C. et al., 2023, ApJ, 944, L14
Woo J.-H., Urry C. M., 2002, ApJ, 579, 530
Yoshizawa M., Wakamatsu K., 1975, A&A, 44, 363
Yu S.-Y., Ho L. C., 2018, ApJ, 869, 29
Yu S.-Y., Ho L. C., 2019, ApJ, 871, 194
Zibetti S., Charlot S., Rix H.-W., 2009, MNRAS, 400, 1181

This paper has been typeset from a TEX/LATEX file prepared by the author.